Neurochemical Research (2019) 44:1475–1493
https://doi.org/10.1007/s11064-019-02781-w

ORIGINAL PAPER

In Vivo Phenotyping of Familial Parkinson's Disease with Human Induced Pluripotent Stem Cells: A Proof-of-Concept Study

Ourania Zygogianni[1,2] · Nasia Antoniou[1] · Maria Kalomoiri[1] · Georgia Kouroupi[1] · Era Taoufik[1] · Rebecca Matsas[1]

Received: 26 November 2018 / Revised: 14 March 2019 / Accepted: 15 March 2019 / Published online: 15 April 2019

Abstract

Parkinson's disease (PD) is the second most common neurodegenerative disorder. We have previously developed a disease-in-a-dish model for familial PD using induced pluripotent stem cells (iPSCs) from two patients carrying the p.A53T α-synuclein (αSyn) mutation. By directed differentiation, we generated a model that displays disease-relevant phenotypes, including protein aggregation, compromised neurite outgrowth, axonal neuropathology and synaptic defects. Here we investigated the in vivo phenotypes of iPSCs, derived from one patient, after transplantation in a lesion mouse model established by unilateral intrastriatal 6-hydroxydopamine injection in the immunosuppressed NOD/SCID strain. Immunohistochemistry revealed that despite the disease-related characteristics that mutant cells displayed when maintained up to 70 days in vitro, they could survive and differentiate in vivo over a 12-week period. However, some differences were noted between patient-derived and control grafts, including a significant rise in αSyn immunoreactivity that might signal a first step towards pathology. Moreover, control-derived grafts appeared to integrate better than PD grafts within the host tissue extending projections that formed more contacts with host striatal neurons. Our data suggest that the distinct disease-related characteristics which p.A53T cells develop in vitro, may be attenuated or take longer to emerge in vivo after transplantation within the mouse brain. Further analysis of the phenotypes that patient cells acquire over longer periods of time as well as the use of multiple iPSC clones from different patients should extend our current proof-of-concept study and provide additional evidence for in vivo disease modeling.

Keywords Dopaminergic neurons · In vitro disease modeling · Cell transplantation · 6-OHDA striatal lesions · Motor behavior · Alpha-synuclein

Introduction

The groundbreaking technology of human induced pluripotent stem cells (hiPSC) has opened up new prospects for understanding human biology and disease. It has prompted the creation of in vitro patient-derived models of disease and raised hopes for autologous cell replacement therapies [1]. Parkinson's disease (PD) is the second most common neurodegenerative disorder associated with progressive loss of striatal-projecting dopaminergic neurons of the substantia nigra pars compacta, resulting in debilitating motor deficits [28]. Even though it is still unknown whether dopamine neuron degeneration is an initial disease feature or the inevitable consequence of multiple dysfunctions throughout the brain, it represents a common pathological manifestation in PD and is responsible for many of the clinical symptoms. A major neuropathological hallmark of PD is the presence of intracellular protein aggregates in the cell bodies and neurites

Special issue in honor of Prof Anthony J Turner.

Electronic supplementary material The online version of this article (https://doi.org/10.1007/s11064-019-02781-w) contains supplementary material, which is available to authorized users.

✉ Era Taoufik
etaoufik@pasteur.gr

✉ Rebecca Matsas
rmatsa@pasteur.gr

[1] Laboratory of Cellular and Molecular Neurobiology – Stem Cells, Department of Neurobiology, Hellenic Pasteur Institute, 127 Vassilissis Sofias Avenue, 11521 Athens, Greece

[2] Faculty of Nursing, University of Athens, 11527 Athens, Greece

of affected neurons, respectively termed Lewy bodies and Lewy neurites, which are mainly composed of α-synuclein (αSyn). This is a small pre-synaptic protein whose physiological function is still under investigation, yet its pathological involvement in PD is widely accepted [53]. αSyn is the major sporadic PD linked gene [51], whereas point mutations [36] and multiplications [5] of the locus cause an autosomal dominant form of the disease, often characterized by early onset and a generally severe phenotype. The best-studied αSyn mutation is p.A53T (G209A in the SNCA gene), first identified in families of Italian and Greek ancestry [22, 34, 37]. Other PD-associated monogenic mutations include the genes PINK1, Parkin, LRRK2, DJ-1, ATP13A2 and VPS35 [38]. Although the majority of PD cases are sporadic, studies on familial forms that are clinically and neuropathologically similar to sporadic PD have assisted in gaining insights into PD etiopathology.

In recent years the advent of hiPSC has provided a valuable means for modeling PD in vitro using cellular systems derived from patient cells [4, 6, 7, 14, 23, 29, 31, 33, 40, 43–45, 48, 52]. Thus a number of studies have shown disease-relevant characteristics in patient hiPSC-derived neurons in vitro that include increased sensitivity to oxidative and nitrosative stress [4, 33, 43], mitochondrial deficits [6, 43, 44], axonal defects and synaptopathy [23, 45]. Nevertheless, whether the vulnerability of hiPSC-derived PD neurons is also retained in an in vivo setting after transplantation in the rodent brain, has been addressed in a limited number of studies. In an initial study, engrafted neurons generated from sporadic PD patients were shown to survive in vivo in the 6-hydroxydopamine (6-OHDA) model of PD in rats, even though only few donor-derived neurons projected their axons towards the dopamine-depleted host striatum [11]. These observations were recently confirmed in a primate model of PD where sporadic PD patient hiPSC-derived neurons survived and extended neurites into the host striatum [17]. This effect was consistent regardless of whether the cells were derived from patients with idiopathic PD or from healthy individuals [18]. Surprisingly similar studies using hiPSC-derived neurons from patients with familial forms of PD have lagged behind, despite the large number of mutation-carrying hiPSC lines that have been generated for in vitro disease modeling. In the only study reported so far, hiPSC-derived neurons carrying the LRRK2-G2019S mutation were found to survive in vivo in the mouse brain, but also to up-regulate αSyn which is believed to be a first step towards induction of pathology [13].

Here we sought to investigate the phenotype of p.A53T-patient-derived neurons in vivo vis-à-vis control neurons derived from a healthy individual after transplantation in a 6-OHDA lesion mouse model developed in the immunosuppressed NOD/SCID strain. We have recently reported the generation and characterization of a "disease-in-a dish" model of hiPSC-derived neurons from PD patients carrying the p.A53T-αSyn mutation [23]. In this model, comprising dopaminergic, GABAergic and glutamatergic cells, p.A53T-neurons display a number of disease-associated features, including protein aggregation, compromised neuritic outgrowth and contorted or fragmented axons with swollen varicosities containing αSyn and Tau. Moreover, mutant neurons show disrupted synaptic connectivity and widespread transcriptional alterations in genes involved in synaptic signaling. Interestingly, small molecules that target αSyn and prevent its aggregation [60] could rescue the impaired synaptic connectivity and axonal neuropathology of p.A53T neurons, providing a direct link between the identified disease-associated phenotypes and pathological αSyn [23]. Here we further explored the in vitro properties of these p.A53T-hiPSC derived from one patient and a healthy control, differentiated to the dopaminergic lineage, and investigated if they could survive and differentiate after transplantation in the host brain. We demonstrate that patient cells start to display initial pathological characteristics in vivo over a 12-week period and provide proof-of-concept that this approach may be useful for in vivo disease modeling.

Experimental Procedures

Dopaminergic Differentiation of Human iPSCs

The PD patient-derived p.A53T-hiPSC and healthy donor control lines used in this study were generated and characterized as previously described (Table 1; Kouroupi et al. [23]). For dopaminergic differentiation a floor-plate induction protocol was applied [25] with minor modifications. Immediately preceding differentiation, hiPSC colonies were dissociated into a single cell suspension using accutase (Life Technologies) and were plated (40,000 cells per cm^2) on

Table 1 Cell line information used in the present study regarding donor age at sampling, gender and reprogramming method

iPSC lines genetic mutation	Age of skin biopsy/gender	Reprogramming method	Reference
Control SNCA-WT	43, Male	OSKM[a] retrovirus	Kouroupi et al. [23]
PD SNCA-G209A	51, Male	OSKM retrovirus	Kouroupi et al. [23]

[a]Oct3/4, Sox2, Klf4 and c-Myc

matrigel (BD Biosciences) in DMEM/ F12 medium containing 15% knockout serum replacement (KSR), 2 mM Glutamax and 10 mM β-mercaptoethanol. Floor-plate induction was performed by addition of LDN193189 (100 nM, Stemgent), SB431542 (10 mM, Tocris), SHH C24II (100 ng/ml, R&D), purmorphamine (2 mM, Stemgent), FGF8 (100 ng/ml, R&D) and CHIR99021 (CHIR; 3 mM, Stemgent) as summarized in Fig. 1a. On day 5 of differentiation (5 days in vitro, DIV), KSR medium was gradually changed to N2 medium (25%, 50%, 75%). On 11 DIV, the medium was changed to Neurobasal/B27/Glutamax (Invitrogen) supplemented with BDNF (brain-derived neurotrophic factor, 20 ng/ml; R&D), GDNF (glial cell line-derived neurotrophic factor, 20 ng/ml; R&D), TGFβ3 (transforming growth factor type β3, 1 ng/ml; R&D), ascorbic acid (0.2 mM, Sigma), dibutyryl cAMP (0.5 mM; Sigma-Aldrich), and DAPT (10 mM; Tocris) for 9 days (differentiation medium). At 20 DIV, cells were dissociated using accutase and replated at high density (300,000 cells per cm^2) on dishes pre-coated with polyethylenimine (PLE; 15 mg/ml; Sigma-Aldrich)/ laminin (1 mg/ml)/ fibronectin (2 mg/ml) in differentiation medium until the desired maturation stage.

Magnetically Activated Cell Sorting (MACS) of PSA-NCAM-Positive Cells

For enrichment in PSA-NCAM-positive immature neurons, hiPSC-derived cells driven to differentiate to the dopaminergic lineage were incubated at 28 DIV with 10 mM Y27632 (ROCK inhibitor) for 1 h to prevent cell death. MACS was performed according to the manufacturer's instructions (Miltenyi Biotech). Accutase-dissociated cells were treated with 1% BSA followed by incubation with anti-PSA-NCAM magnetic Microbeads (Cat. Number 130-092-966) for 15 min at 4 °C. After extensive washing, the cell suspension was loaded on the separation column (MS column) attached to a magnetic stand. Labeled cells were retained and after removal of the column from the magnetic separator, they were eluted with differentiation medium, counted and replated. After 2 days (30 DIV) cells were either analyzed by immunofluorescence and RT-qPCR or were dissociated to single cell suspension for transplantation. Some cultures were maintained in differentiation medium for longer periods of time and were analyzed by immunofluorescence, electrophysiology and calcium imaging at the indicated time points. Cultures grown for more than 50 DIV were replated on a mouse astrocyte feeder layer [23].

RNA Isolation, cDNA Synthesis and qPCR

Total RNA was extracted from cell pellets using the TRIzol Reagent (Life Technologies). Following digestion with DNase I, 1 μg of total RNA was used for first strand cDNA synthesis with the ImProm-II Reverse Transcription System (Promega) according to the manufacturer's instructions. Quantitative PCR analyses were carried out in a Light Cycler 96 (Roche) Real time PCR detection system using KAPA SYBR FAST qPCR Master Mix (KapaBiosystems). The housekeeping gene GAPDH was used as a reference. The primers used are listed in Supplementary Table 1.

Immunofluorescence

Cells were fixed with 4% paraformaldehyde (Sigma-Aldrich) for 20 min at room temperature. Samples were blocked with 0.1% Triton X- 100 (Sigma-Aldrich) and 5% donkey serum in PBS for 30 min and were subsequently incubated with primary antibodies (listed in Supplementary Table 2) at 4 °C overnight, followed by incubation with appropriate secondary antibodies (Molecular Probes, Thermo Fisher Scientific) conjugated to AlexaFluor 488 (green), 546 (red) or 647 (blue), for 2 h at room temperature. Coverslips were mounted with ProLong Gold antifade reagent containing DAPI (Cell Signaling). Digital images were acquired using a Leica TCSSP8 confocal microscope (LEICA Microsystems) and analyzed using ImageJ software (NIH). Protein aggregates were detected with the PROTEOSTAT Aggresome Detection Kit (Enzo) [49] followed by immunolabeling for either DCX or TH. As positive control for the assay we treated healthy iPSC-derived neurons with either DMSO or the proteasome inhibitor MG-132 (10 μM) for 6 h or 18 h and visualized sequestered fluorescently labeled protein cargo (not shown). For quantification, the number of aggregates per cell in DCX+ or TH+ neurons was counted using ImageJ on twenty randomly selected fields from two independent experiments. Quantification is shown in a box with whisker plot, where the line inside the box represents the median, while the bars outside the box represent the minimum and maximum values (spread) of all data. Analysis and quantification of TH axon degeneration was performed as previously described [23]. Briefly, the number of TH+ spots in fragmented axons was counted using ImageJ on twenty randomly selected fields and the ratio between the number of spots and the total TH+ staining area was designated as TH axon degeneration index.

6-OHDA Lesioned Mice and Cell Transplantation

All animal procedures were performed in strict compliance with the European and National Laws for Laboratory Animal Use (Directive 2010/63/EU and Greek Law 56/2013), according to FELASA recommendations for euthanasia and the Guide for Care and Use of Laboratory Animals of the National Institutes of Health. All protocols were approved by the Institutional Animal Care and Use Committee of the Hellenic Pasteur Institute (Animal House Establishment

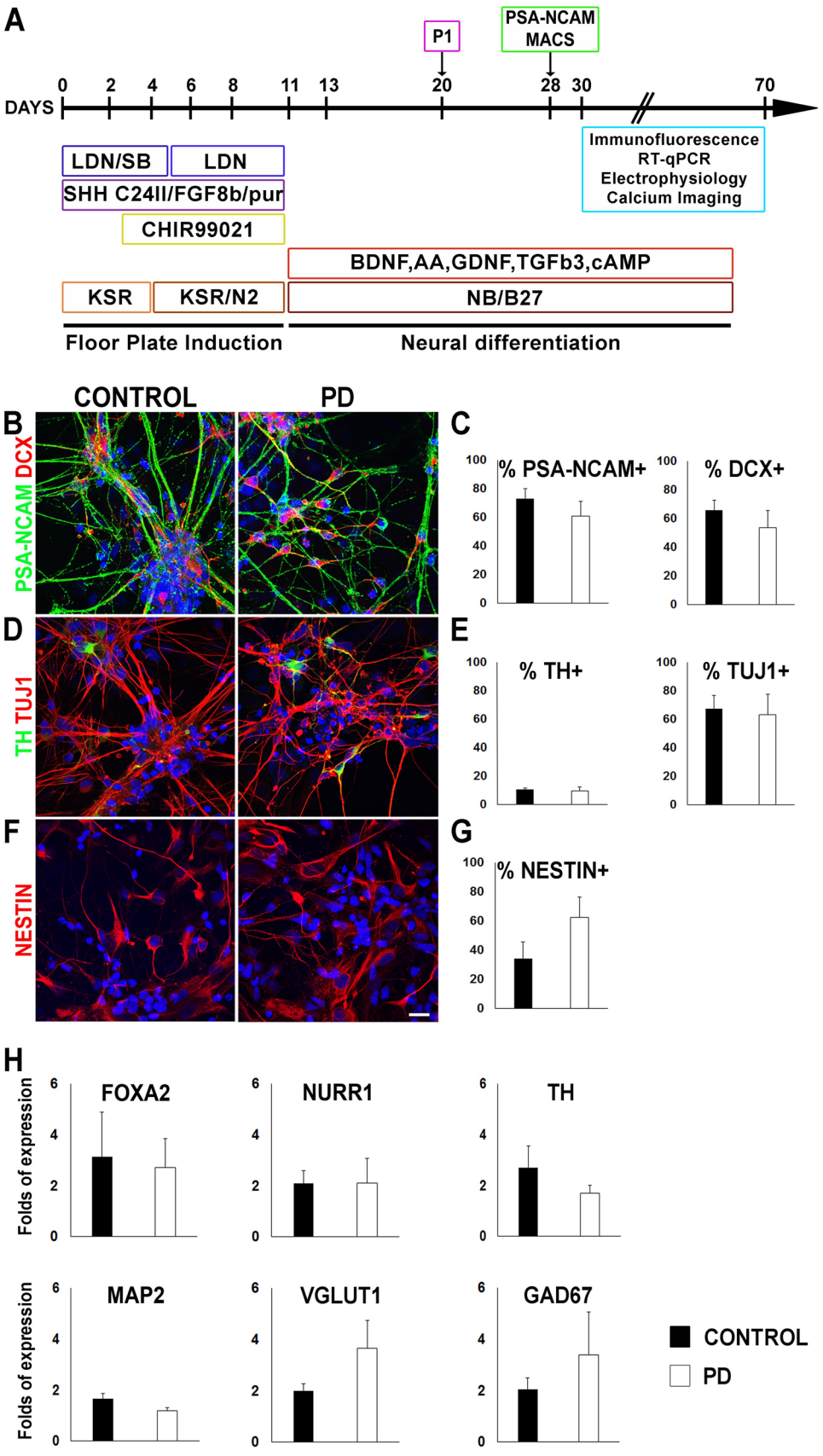

Fig. 1 Dopaminergic differentiation of hiPSC-derived cells. **a** Schematic representation of the differentiation protocol used and timeline of analysis, following MACS isolation at 28 DIV. **b, d** Double immunofluorescence of control and PD cells at 30 DIV for: **b** PSA-NCAM (green) and doublecortin (red, DCX); **d** TH (green) and βIII-tubulin (TUJ1, red). Cell nuclei are in blue. **c, e** Quantification of positive cells for each marker in control versus PD cultures is shown as percentage of total nuclei. **f** Immunofluorescence for the neural progenitor marker Nestin (red) and **g** quantification of Nestin-positive cells as percentage of total nuclei. Data represent mean ± SEM (n = 3–5), P > 0.05. Scale bar, 10 µm. **h** RT-qPCR analysis of mRNA expression at 30 DIV for the indicated neuronal and dopaminergic lineage markers. Data represent mean ± SEM (n = 3)

Code: EL 25 BIO 013) and the License No 5677/25-09-2012 for experimentation was issued by the Greek authorities (Veterinary Department of Athens Prefecture). The preparation of this manuscript was made in compliance with ARRIVE guidelines for reporting animal research. Male NOD.CB17-Prkdcscid/NCrHsd mice 9–10 weeks old were anesthetized using gaseous isoflurane (2–5% in 2:1 O_2:N_2) and received 2 × 1 µl unilateral stereotactic injections of 4 µg/µl 6-hydroxydopamine (6-OHDA, Sigma) dissolved in physiological saline containing 0.02% ascorbic acid. Infusions were delivered over 1 min via a 30 gauge stainless steel cannula. Lesions were made in the right mid-striatum (AP = + 0.5 mm to bregma, ML = + 1.8 mm, DV = − 3.0 and − 3.5 mm). The cannula was left in place for a further 2 min, before being slowly removed. The wound was cleaned and closed with sutures. Animals were monitored daily and for the following 10 days received subcutaneously 0.5 ml of 0.9% saline/ glucose solution to prevent dehydration. Behavioral tests were performed 14 days after the lesions, when the animals had fully recovered.

Three weeks after 6-OHDA injection PSA-NCAM-enriched cells from control or PD hiPSC lines were stereotactically transplanted in mice. Cells were dissociated with accutase and re-suspended in cold HBSS (Invitrogen) at a density of 100,000 cells/µl. Mice received 2 × 1 µl cells at the same coordinates that the lesions were made at a rate of 0.5 µl/min.

Behavioral Analysis

Rotational asymmetry was analyzed at 2, 7, 11 and 15 weeks after 6-OHDA lesioning, using a spontaneous activity test (drug-free asymmetry) and after intraperitoneal (i.p) injection of amphetamine (4 mg/kg; drug-induced asymmetry). *Spontaneous activity test*. Limb-use asymmetry was estimated as follows. A transparent cylinder was placed on a piece of transparent plastic to visualize stepping movement from underneath and overall movement from above. The right hindlimb was marked in order to distinguish left from right steps. Sessions were videotaped for 3 min and scored offline to evaluate the number of steps taken by each limb [ipsilateral and contralateral (the impaired paw), forelimb and hindlimb]. The ratio of ipsilateral to contralateral steps was calculated for the forelimbs and hindlimbs [10]. *Amphetamine test*. Amphetamine-induced ipsilateral rotations increase in response to a unilateral lesion. Mice were injected i.p. with 10 mg/kg of d-amphetamine sulphate and were left for 10 min to acclimatize in a plastic box. Rotational activity was measured over a 30 min period [59] and data were expressed as net ipsilateral minus contralateral turns. Mice with > 5 net ipsilateral turns were used for transplantation and were analyzed by immunocytochemistry after a further 12 weeks (mice that received control-derived grafts: n = 5; mice that received PD-derived grafts: n = 3).

Immunohistochemistry

Animals were perfused intracardially with 0.9% saline solution and 4% paraformaldehyde (pH 7.4). Perfused brains were either cryopreserved in 30% sucrose and frozen in OCT compound for obtaining cryostat 20 µm-sections [24] or were embedded in 4% agarose and sectioned (40 µm) on a vibrating microtome (Leica), serially collected. Slices were blocked with 0.1% Triton X-100 (Sigma–Aldrich), 2 mg/ml BSA and 1.5% donkey serum in PBS for 3 h and were subsequently incubated with primary antibodies (Supplementary Table 1) at 4 °C either overnight for cryostat sections or for 3 nights for vibrating microtome sections, followed by incubation with appropriate secondary antibodies (Molecular Probes, Thermo Fisher Scientific) conjugated to AlexaFluor 488 (green), 546 (red) or 647 (blue). Sections were mounted on slides with ProLong Gold antifade reagent containing DAPI (Cell Signaling). Digital images were acquired using a Leica TCSSP8 confocal microscope (LEICA Microsystems) and analyzed using ImageJ software (NIH). For quantification of the graft area as well as the percentage of cells positive for the different markers, 3–5 slices from each animal were analyzed.

Image Processing and Quantification of Fluorescence Intensity

For the evaluation of the expression levels of human aSyn, single channel stacks of confocal images were acquired under the same settings (constant gain and offset values, 63 × objective, 4 × averaging, 2048 × 2048 pixel resolution, and 1-µm step size). Tile scans were acquired to include the total graft areas. Quantification of fluorescence intensity was performed using ImageJ software by a blind observer, after free-hand selection of the graft area on the maximum projection image as the region of interest (ROI) and setting the threshold at a constant value. The number of thresholded pixels per graft area (μm^2) were averaged from single images of the confocal stack. Three mice were analyzed in each group and the values from 2 sections were averaged per mouse.

Quantification of Graft-Derived Human Synaptophysin (HSYP) Contacts on DARRP32-Positive Striatal Medium Spiny Neurons of the Host

The quantification was performed as follows: 5 digital images (63X lens, zoom x 3, constant gain and offset values, 4 × averaging, 2048 × 2048 resolution, 0.5 µm step size)

were acquired at the graft-host tissue interphase. Within every image, 4 representative regions of interest (ROI) were selected and the number of contacts between HSYP and DARPP32 was counted by a blind observer. Because simultaneous quantification of HSYP and human nuclei or human cytoplasmic antigen was not possible due to the fact that all antibodies were raised in mice, to minimize differences arising from variations in the number of grafted neurons per animal we took special care to perform measurements only at the graft-host tissue interphase and in representative regions of interest (ROI) with similar synaptophysin immunofluorescence intensity. Five control-derived and three PD-derived animals were analyzed and the values from 2 sections were averaged per mouse.

Electrophysiology

Patch-clamp recordings were performed as previously described [23]. Whole-cell voltage clamp recordings were made from hiPSC-derived neurons at 55–60 DIV. The pharmacological inhibitors tetrodotoxin (TTX; final concentration 1 µM) and tetraethylammonium (TEA; 10 mM) were applied to block voltage-gated sodium and potassium channels, respectively. Data were acquired at room temperature (22–24 °C) using an EPC9 HEKA amplifier and an ITC-16 acquisition system with a patchmaster software (HEKA). Data analysis was performed using OriginPro 8 (OriginLab Software).

Calcium Imaging

At 55–60 DIV hiPSC-derived neurons were incubated with culture medium containing 3 µM Fluo-3 (Molecular Probes) for 30 min at 37 °C. After washing with extracellular solution (mM: 140 NaCl, 2.8 KCl, 2 $CaCl_2$, 4 $MgCl_2$, 20 HEPES, 10 glucose, pH 7.4–7.5), cells were placed into fresh extracellular solution and equilibrated in the microscope chamber at 5% CO_2, 70–75% humidity, 37 °C for 30 min. Cells were excited at 488 nm with a fluorescein isothiocyanate (FITC) filter; the fluorescence signals were recorded at 10 frames/sec using a fluorescence Olympus Time lapse IX81 Cell-R microscope. From each field, 20–30 cells were selected for analysis of Ca^{2+} responses using ImageJ software. The amplitude of fluorescence signals for each region of interest (ROI) was presented as relative fluorescence changes (DF/F) after background subtraction. The Ca^{2+} transient frequency and amplitude were counted manually over a 5-min period.

Statistical Analysis

All in vitro experiments were replicated at least three times and data from parallel control and PD cultures were acquired. The in vivo data were obtained from two independent experiments. All data represent mean ± standard error of the mean (SEM). Statistical analysis was performed in Microsoft Office Excel 2013. In each case, comparisons between the two groups (control and PD) were performed using the Student's t-test or the Mann–Whitney Test as indicated. Probability values less than 0.05 ($P < 0.05$) were considered significant.

Results

Dopaminergic Differentiation and Characterization of PSA-NCAM Enriched PD Cultures

Several hiPSC differentiation protocols have been developed to improve dopaminergic neuron specification and their in vivo performance, particularly in terms of avoiding cellular overgrowth [20, 25, 45, 54, 62]. In this study, we reasoned that an enriched population of neuronal cells differentiated to the dopaminergic lineage, consisting of progenitors and early neurons with restricted proliferative capacity, would be appropriate for transplantation studies [8, 11, 17, 54]. To this end, we applied a floor plate induction protocol [25] to differentiate a previously generated p.A53T-hiPSC (PD) line by comparison to a healthy donor (control) line [23] towards the dopaminergic lineage (Fig. 1a). At the end of floor plate induction (11 DIV), LMX1A/FOXA2-positive dopaminergic precursors were derived (Suppl. Fig. 1). At this stage practically all cells were LMX1A-positive floor plate precursors and approximately half were also FOXA2-positive in agreement with a dopaminergic fate (percentage of FOXA2-positive cells: control 44.01 ± 5.67%, n = 3; PD 48.63 ± 7.32%, n = 3). Engraftable neurons are obtained with this protocol after 25 DIV [25]. To avoid cellular overgrowth, further enrichment in PSA-NCAM-positive neuronal cells was achieved by MACS isolation on the basis of PSA-NCAM immunoreactivity at 28 DIV (Fig. 1a). Two days later at 30 DIV, sorted cells were analyzed by immunofluorescence for the immature neuronal markers PSA-NCAM and Doublecortin (DCX) (Fig. 1b). Quantification (Fig. 1c) revealed that 60–73% of the cells in the culture expressed PSA-NCAM and 53–65% expressed the immature neuronal marker DCX with no statistically significant differences between control and PD (For PSA-NCAM: control 73.06 ± 6.89% n = 4; PD 60.88 ± 10.26% n = 5; P = 0.341. For DCX: control 65.60 ± 7.15% n = 4; PD 53.57 ± 12.06% n = 5; P = 0.397). A similar number of cells in the two types of culture expressed the neuronal lineage marker βIII-Tubulin (TUJ1, control 67.35 ± 9.41% n = 4; PD 63.29 ± 14.19% n = 5; P = 0.812). The number of neurons positive for the dopaminergic neuronal marker tyrosine hydroxylase (TH) was approximately 10% (control 10.85 ± 0.97% n = 3; PD 9.86 ± 2.84% n = 4; P = 0.724), which is not surprising as

cells are still at an immature differentiation state at this time point [25] (Fig. 1d, e). A significant proportion of Nestin positive neural progenitors were also present, more in PD cultures, without statistical significance as compared to controls (control 34.17 ± 11.54%, n = 3; PD 62.36 ± 14.14%; n = 3; P = 0.197) (Fig. 1f, g), indicating an overlap between the Nestin- and βIII-Tubulin-positive populations. Proliferating Ki-67 positive cells were less than 10% in both cultures (control 7.16 ± 3.73% n = 4; PD 9.8 ± 5.04%; n = 3, P = 0.683).

RT-qPCR confirmed mRNA expression of the dopaminergic lineage markers FOXA2 (early progenitors), NURR1 (late progenitors) and TH (mature neurons) (Fig. 1h) whilst other neuronal markers, including MAP2 (neuron-specific marker), GAD67 (GABAergic neuron marker) and VGLUT1 (glutamatergic neuron marker) were also detected. Overall no marked differences were apparent between PD and control cultures at 30 DIV, either by immunofluorescence or RT-qPCR analysis.

Appearance of Degenerative Phenotypes in Prolonged Cultures of PD Neurons

Morphological Alterations

Because the differentiation protocol we used in this study was different from that we previously reported in [23], before proceeding to in vivo transplantation we addressed the phenotype of PD cultures maintained for longer periods of time in vitro. When cells were analyzed between 45 and 70 DIV, degeneration signs became apparent. First we noted that DCX-positive cells, which constituted approximately one-third of the total population in both cultures at 47 DIV, exhibited morphological differences between control and PD. PD DCX positive cells had significantly more primary neurites per cell (Fig. 2a, b; control 2.42 ± 0.04 and PD 3.38 ± 0.16, n = 3 per group; *P = 0.029) and an increased number of secondary branches per cell (Fig. 2a). Moreover, intracellular protein aggregates were detected in PD DCX-positive neurons at 70 DIV, as indicated with a fluorescence-based assay for detection of aggregated protein cargo (Fig. 2c and quantification of the number of aggregates per DCX + cell in Fig. 2d; Mann–Whitney Test, control median 0.00, n = 265 and PD median 5.00, n = 173; ****P < 0.00001) Additionally mutant TH-positive cells, which formed a dense network at 70 DIV, displayed dystrophic neurites with swollen varicosities that quite often ended up in fragmented processes (Fig. 2e and quantification of the TH axonal degeneration index in Fig. 2f; Student's t-test, control 3.22 ± 0.81 and PD 43.34 ± 7.41, n = 20 randomly selected fields for each condition; ****P = 0.00003). These features were accompanied by detection of intracellular protein aggregates in PD cells (Fig. 2g and quantification in Fig. 2h; Mann–Whitney Test, control median 1.00, n = 167; PD median 6.00, n = 155; ****P < 0.00001). Immunofluorescence indicated that αSyn was also upregulated in PD cultures (Suppl. Fig. 2A, B). Thus our analysis revealed new phenotypes in p.A53T-neurons related to the morphology of DCX^+ cells, and defective neuropathological characteristics similar to those previously reported, including increased αSyn immunoreactivity, presence of protein aggregates and dystrophic neurites [23].

Electrophysiological Recordings

Because of the neuropathological features noted above, we asked if there were also functional differences between control and PD cultures. Whole-cell patch-clamp recordings were performed to assess the functional maturation of hiPSC-derived neurons between 55 and 60 DIV (Fig. 3). Voltage-clamp recordings demonstrated the presence of transient inward sodium currents and sustained outward potassium currents (representative traces are shown in Fig. 3a) that could be blocked by the Na_v-blocker TTX (1 µM) and K_v-blocker TEA (10 mM), respectively (Fig. 3a). Current–voltage relationship curves show the activation of voltage-gated sodium and potassium channels (Fig. 3b, c). For control and PD hiPSC-derived neurons the passive and active membrane properties were compared. The mean input resistance was 1.011 ± 0.186 GΩ (n = 14) and 1.711 ± 0.397 GΩ (n = 9), respectively (Fig. 3d). Resting membrane potential was − 57.14 ± 5.34 mV (n = 14) and − 74.44 ± 9.59 mV (n = 9) respectively (Fig. 3e). In agreement with our previous observations [23], we did not observe statistically significant differences on active and passive membrane properties between control and PD cells.

Dysregulated Calcium Activity in PD Neurons

We next assessed the integrity of the PD neuronal network using calcium imaging for the first time in these cells, to measure spontaneous Ca^{2+} transients at 55–60 DIV. We observed significantly more spontaneous Ca^{2+} transients in PD as compared to control cultures (Fig. 3f, g; control 0.01 ± 0.002, n = 20; PD 0.04 ± 0.003, n = 33; **** $P = 2.51 \times 10^{-10}$) with significantly larger mean amplitude (Fig. 3h; control 1.70 ± 0.21, n = 22; PD 2.33 ± 0.15, n = 35; * P = 0.02). As calcium dynamics regulate neurite growth and synaptic connectivity [16, 26, 61], our data suggest that the observed alterations in calcium signaling should impact on, and explain, the morphological phenotypes of PD neurons.

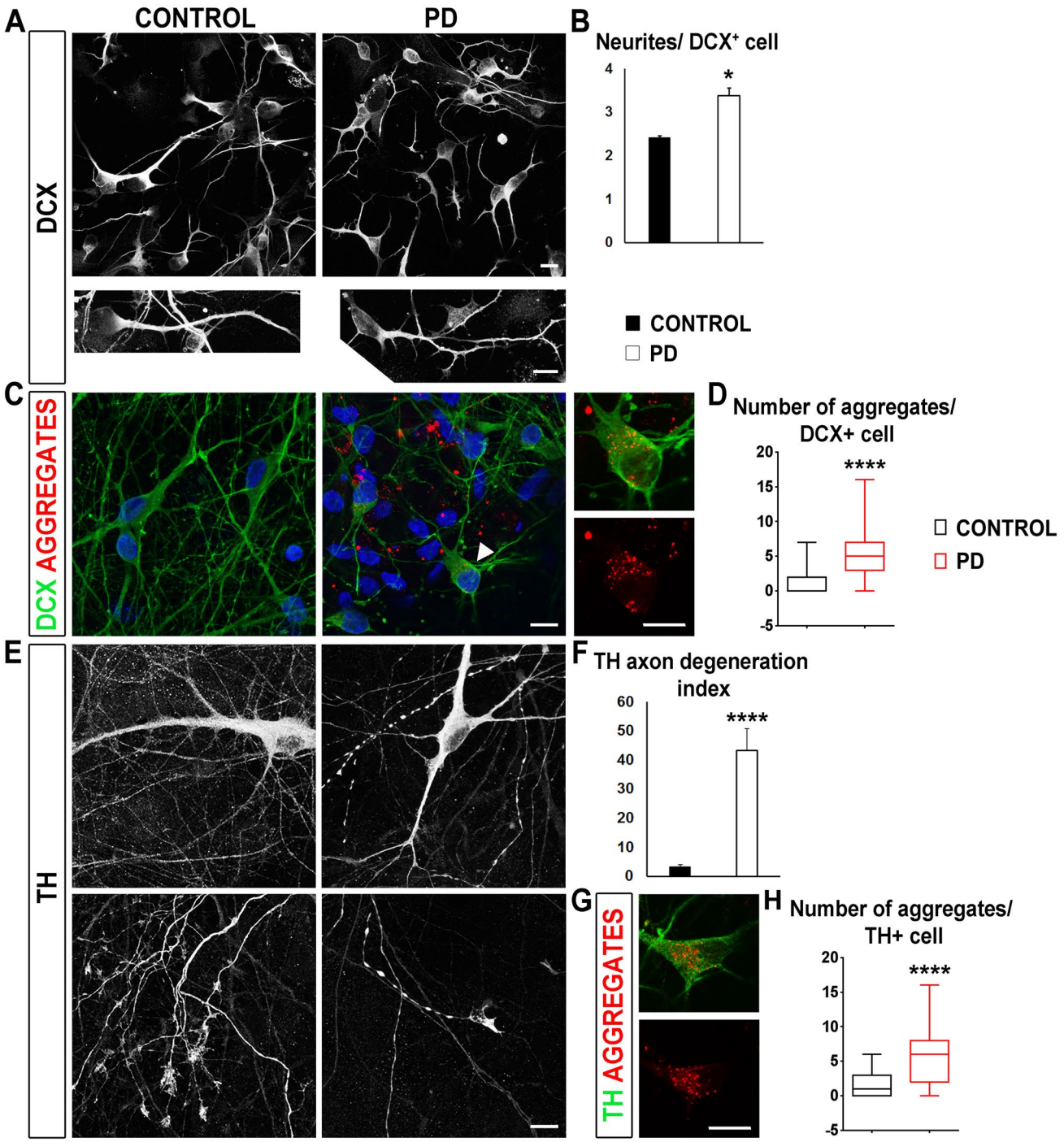

Fig. 2 Pathological phenotypes of hiPSC-derived PD neurons in prolonged cultures. **a** Representative images in upper and at higher magnification in lower panels, illustrating the more branched morphology of DCX-positive cells in PD versus control cultures at 47 DIV. **b** Quantification of the number of total neurites per DCX-positive cell (control 2.42 ± 0.04 and PD 3.38 ± 0.16, n = 3; *P = 0.029). **c** At 70 DIV protein aggregates (aggresomes, red) are detected throughout in PD cultures and intracellularly in DCX-positive cells (green), but not in control cells. **d** Quantification of protein aggregates in DCX-positive cells (Mann–Whitney Test; control median 0.00, n = 265 and PD median 5.00, n = 173; ****P < 0.00001). **e** Immunostaining for TH at 70 DIV shows PD neurites with swollen varicosities (upper panel) that end up in fragmented processes (lower panel). **f** Quantification of axon degeneration index in arbitrary units. Data represent mean ± SEM (Student t-test, control 3.22 ± 0.81 and PD 43.34 ± 7.41, n = 20 randomly selected fields for each condition; ****P = 0.00003). **g** Intracellular protein aggregates detected in PD TH-positive neurons at 70 DIV. Scale bars, 10 µm. **h** Quantification of protein aggregates in TH-positive cells (Mann–Whitney Test; control median 1.00, n = 167; PD median 6.00, n = 155; ****P < 0.00001)

Induction and Characterization of a 6-OHDA Lesion Model in Immunodeficient Mice Reveals Spontaneous Recovery of Motor Function

To investigate the in vivo phenotype of PSA-NCAM-enriched hiPSC-derived cells at 30 DIV, we developed a 6-OHDA lesioned mouse model in the NOD/SCID strain that supports xenograft survival [12]. Indeed previous studies have shown that lesions increase the survival and integration of transplanted cells within the host brain [2]. Even though our aim was to use this lesion model as a means for sustaining graft survival, and not for therapeutic purposes, we considered necessary to characterize its properties for the duration of the experiment. A unilateral lesion was induced by intrastriatal injection of 6-OHDA in 9–10 week old mice and the resulting functional deficit was confirmed 2 weeks later using drug-induced and drug-free behavioral analysis (Fig. 4a–c). Amphetamine-induced rotational asymmetry was assessed over a 15-week period (Fig. 4a). Surprisingly, although 6-OHDA injection led to significantly increased ipsilateral turns per min at 2 weeks post injection (6-OHDA 8.64 ± 0.76; $n = 16$; saline 0.48 ± 0.72 turns per min; $n = 13$; ****$P = 2.25 \times 10^{-8}$), ipsilateral turns were notably decreased over time. At 7 weeks, turns in the 6-OHDA group were 3.93 ± 0.43 per min ($n = 5$) versus 0.78 ± 1.02 per min in the saline group ($n = 6$), *$P = 0.025$. Finally, at 11 and 15 weeks values were not substantially different between the two groups (11 weeks: 6-OHDA 2.82 ± 0.71 turns, $n = 6$; saline 1.09 ± 0.79 turns, $n = 5$, $P = 0.138$; and 15 weeks; 6-OHDA 0.47 ± 0.39 turns, $n = 6$ and saline -0.32 ± 0.87 turns, $n = 4$, $P = 0.453$).

Spontaneous forelimb and hindlimb activity was also measured at the same time points (Fig. 4b, c). Preference for ipsilateral steps was significantly higher in the 6-OHDA group as compared to the saline group at 2 weeks (forelimbs: 6-OHDA 1.63 ± 0.10 ipsi/contralateral steps per min, $n = 12$; saline 1.07 ± 0.06, $n = 6$; ***$P = 0.0002$; hindlimbs: 6-OHDA 2.68 ± 0.29, $n = 10$; saline 1.07 ± 0.24, $n = 6$; ***$P = 0.0007$) with the difference leveling out thereafter both for forelimbs (at 7 weeks: 6-OHDA 0.94 ± 0.03 $n = 4$; saline 1.06 ± 0.03, $n = 4$; *$P = 0.037$; at 11 weeks: 6-OHDA 0.86 ± 0.05, $n = 4$; saline 1.03 ± 0.07, $n = 4$; $P = 0.091$; at 15 weeks 6-OHDA 0.94 ± 0.06, $n = 4$; saline 1.13 ± 0.06, $n = 4$; $P = 0.065$) and hindlimbs (at 7 weeks: 6-OHDA 1.44 ± 0.17, $n = 5$; saline 1.05 ± 0.31, $n = 4$; $P = 0.328$; at 11 weeks: 6-OHDA 1.32 ± 0.21, $n = 5$; saline 1.03 ± 0.14, $n = 4$; $P = 0.289$ and at 15 weeks 6-OHDA 1.15 ± 0.16, $n = 5$; saline 0.85 ± 0.19, $n = 4$, $P = 0.258$). These analyses revealed a spontaneous behavioral recovery in the lesioned animals, which impeded assessment of functional improvement following transplantation.

At the immunohistochemical level, loss of TH-positive neurons in the substantia nigra was validated at 3 weeks post-lesioning (Fig. 2d). A 65.5% loss was observed (Fig. 4e; saline $100 \pm 6.03\%$, $n = 3$; 6-OHDA $34.51 \pm 4.84\%$, $n = 3$; **$P = 0.0011$) which resulted in an extensive striatal dopaminergic denervation (Fig. 4f). Although loss of TH-positive neurons in the substantia nigra remained stable over 15 weeks (60.2% loss, saline $100 \pm 16.61\%$, $n = 3$, 6-OHDA $39.83 \pm 0.7\%$, $n = 3$; *$P = 0.022$), striatal dopaminergic reinnervation was observed (Fig. 4f), in agreement with the concurrent behavioral recovery. Our data indicate extensive sprouting of undamaged TH fibres within the ipsilateral striatum or/and a probable cross-hemispheric compensatory mechanism [9], and highlight the limitations of using the NOD/SCID 6-OHDA model in therapeutic transplantation paradigms.

In Vivo Engraftment of hiPSC-Derived PD Cells

To investigate their phenotypic characteristics in vivo, control and PD hiPSC-derived PSA-NCAM-enriched cells (30 DIV) were transplanted 3 weeks after 6-OHDA injection and immunohistochemical analysis followed after another 12 weeks (Fig. 5a). Analysis of grafted animals was performed by immunohistochemistry. Both control and PD cells managed to survive in the host striatum, as indicated by human-specific cytoplasmic marker staining, and formed well-defined grafts without signs of cellular overgrowth (Fig. 5b). Quantification of the grafted area (mean area in μm^2 from 3 to 7 sections/animal) and the number of human nuclei (HuNu) per section (mean number from 3 to 5 sections/animal) revealed non-significant differences between control and PD grafts (Fig. 5d; graft area: control $164.48 \pm 83.52 \times 10^3$ μm^2, $n = 5$; PD $76.68 \pm 15.7 \times 10^3$ μm^2, $n = 3$; $P = 0.359$; and Fig. 3e; HuNu/ section: control 543.66 ± 182.14, $n = 5$; PD 279.06 ± 180.33, $n = 3$; $P = 0.349$). The host immunological response was also investigated at 12 weeks post-transplantation by immunofluorescence. Control and PD grafts were surrounded by host Iba1-positive macrophage/microglial cells (Suppl. Fig. 3A) whilst activated CD68-positive macrophage/microglia had infiltrated within the grafts in similar numbers between control and PD (Suppl. Fig. 3B, C; control 129 ± 21.44, $n = 5$; PD 156 ± 50.17, $n = 3$; $P = 0.653$). Such CD68-positive activated cells were not evident outside the grafts.

Further immunohistochemical analysis at 12 weeks showed that many of the grafted cells were TUJ1-positive neurons (Fig. 5e, f; control $37.59 \pm 13.44\%$, $n = 5$; PD $19.09 \pm 0.28\%$, $n = 3$; $P = 0.241$), few were TH-positive dopaminergic neurons (< 1%) whilst a subpopulation still expressed the neural progenitor cell marker Nestin (Fig. 5i, j; control $32.64 \pm 5.81\%$, $n = 5$; PD $44.72 \pm 10.68\%$, $n = 3$; $P = 0.394$). The expression of the immature neuronal marker DCX was significantly higher in PD derived grafts as compared to control (Fig. 5g, h; control $16.07 \pm 0.89\%$, $n = 5$;

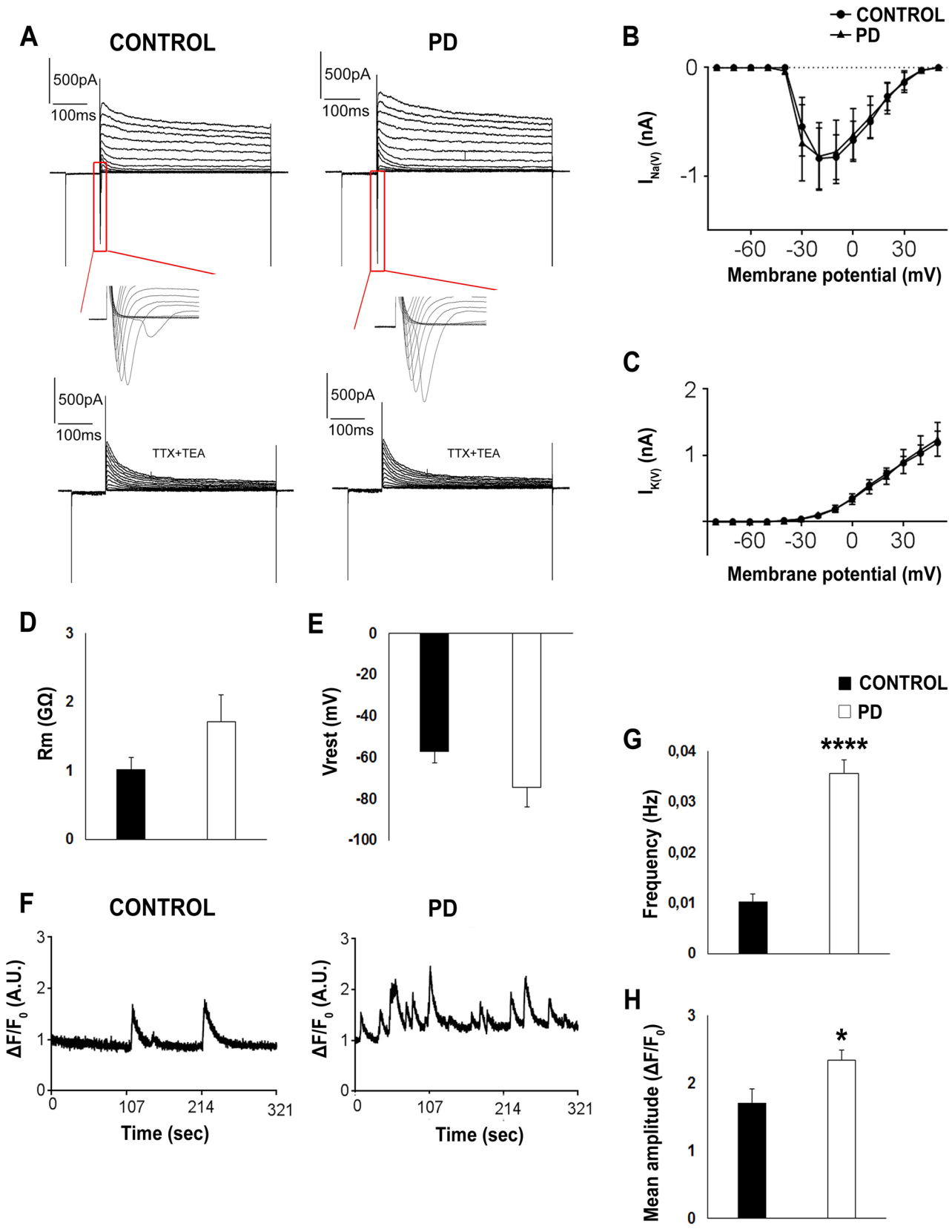
A
CONTROL
PD
500pA
100ms
TTX+TEA
B
CONTROL
PD
$I_{Na(V)}$ (nA)
Membrane potential (mV)
C
$I_{K(V)}$ (nA)
Membrane potential (mV)
D
Rm (GΩ)
E
Vrest (mV)
F
CONTROL
PD
ΔF/F0 (A.U.)
Time (sec)
G
CONTROL
PD
Frequency (Hz)
****
H
Mean amplitude (ΔF/F0)
*

◂**Fig. 3** Electrophysiological properties and spontaneous calcium transients in control and PD neurons. **a** Representative traces of voltage clamp recordings showing fast inward currents followed by long-lasting outward currents, due to voltage steps in 10 mV increments. The inset shows a high magnification view of the inward current. Following initial recording, cells were perfused with 1 μM TTX to block Na^+ currents and with 10 mM TEA (tetraethylammonium) to block K^+ currents. **b, c** The mean current–voltage relations of inward Na^+ currents [$I_{Na(V)}$, (**b**)] and outward K^+ currents [$I_{K(V)}$, (**c**)] under basal conditions show no difference between control and PD neurons. Passive membrane properties: **d** membrane input resistance (Rm) and **e** resting membrane potential (Vrest) show no difference between control and PD neurons. **f** Representative Fluo-3 traces of spontaneous Ca^{2+}- transients (A.U.=arbitrary units), normalized to the average response from the first 40 s of recording. **g** PD neurons displayed a higher frequency (Hz) of Ca^{2+} spikes (control 0.01 ± 0.002, n = 20; PD 0.04 ± 0.003, n = 33; **** $P = 2.51 \times 10^{-10}$) and **h** larger spike amplitude (sec) (control 1.70 ± 0.21, n = 22; PD 2.33 ± 0.15, n = 35; * P = 0.02)

PD 47.28 ± 2.88%, n = 3; **P = 0.009). Astrocytic differentiation was not detected in the grafted cells (not shown). Interestingly, using an antibody against the human protein we noted extensive αSyn immunoreactivity in PD grafts whilst control grafts exhibited much lower αSyn (Fig. 6a). Quantification revealed significantly increased αSyn immunofluorescence intensity in PD-derived grafts as compared to control-derived grafts (Fig. 6b; control 36.744 ± 16.825 pixels/ μm^2, n = 3; PD 207.389 ± 28.466 pixels/ μm^2, n = 3; *P = 0.014), indicating a first step towards induction of pathology. Human αSyn immunoreactivity was not detected outside the grafts, suggesting no spreading to host cells at this time point.

Despite the rather limited differentiation of human neurons at 12 weeks in vivo, application of a human-specific antibody against the synaptic vesicle protein synaptophysin (HSYP), showed widespread immunoreactivity throughout the grafts (Fig. 7a). Double labeling for HSYP and DARPP32 that marks the host striatal medium spiny neurons, revealed an intercalated control graft-to-host interphase as opposed to the sharp boundaries demarcating the PD graft-to-host interphase (Fig. 7b). This suggests that control grafts may integrate better in the host tissue. In support, quantification of $HSYP^+$ contacts onto $DARPP32^+$ neurons in the graft interphase revealed that PD derived cells formed significantly less contacts than control (Fig. 7c; 150.6 ± 21.39, n = 5; PD 85.07 ± 14.73, n = 3;*P = 0.045).

Discussion

A decade ago improved neurodegenerative disease modeling was largely dependent on the development of novel animal models in an effort to recapitulate more faithfully human pathology. Nowadays disease modeling can be performed in a human setting and in a patient-specific manner using hiPSC-derived systems. Despite limitations arising from patient variability, experimental design and data interpretation, the use of hiPSCs has been instrumental in uncovering new disease phenotypes and tracking cellular responses to drugs (for review see Taoufik et al. [55]). To date a large number of hiPSC-based models have been developed by directed differentiation of patient-derived hiPSCs to the appropriate neuronal phenotypes. Especially for PD, attempts have largely focused on the generation of midbrain dopaminergic neurons with the prospect of utilizing them for transplantation therapies [8, 17, 54]. As a result several protocols have been developed with varying efficiency, whilst not all hiPSC clones are capable to differentiate equally well to a particular neuronal population, in this case into dopaminergic cells, even when the same protocol is used [25, 30, 46, 54].

Along this course, we generated several hiPSC lines from two patients with familial PD, carrying the p.A53T αSyn mutation. We thus developed a robust PD model characterized in vitro by protein aggregates, severe axonal neuropathology and defective synaptic connectivity [23]. Importantly, these disease-related characteristics could be reverted by small molecules that target αSyn and prevent its aggregation. In the absence of isogenic gene-corrected control lines, the protective effects of these small molecules provide a direct link between the disease-associated phenotypes and pathological αSyn [23]. The aim of the present study was to investigate the phenotype of these cells in vivo after transplantation in the mouse brain and investigate if the vulnerability of hiPSC-derived PD neurons is retained in an in vivo setting or whether it might be rescued under the supportive influence of the host environment. To this end, we directed p.A53T-hiPSC and corresponding control lines [23] to differentiate to the dopaminergic lineage by applying an efficient floor plate induction protocol that yielded approximately 50% LMX1a/FOXA2-positive progenitors at 11 DIV, a percentage compatible with previous reports [54]. To remove unwanted cells that might cause graft overgrowth, we performed an enrichment in PSA-NCAM-expressing cells, which is known to result in a neuronal population with constrained proliferation potential and enhanced transplantation efficacy [19, 27, 39]. This work is the first description of an in vivo assessment of patient-derived cells carrying the p.A53T mutation, with the limitation that a single clone from a patient and a control were used. It therefore represents a proof-of concept study of the survival and behavior of the mutant cells in the lesioned striatum of immunocompromised mice. Ultimately, the generation and use of isogenic gene-corrected lines should offer a more solid basis for in vivo modeling of p.A53T pathology.

Because in the current study we applied a different differentiation protocol to that previously reported in [23], we deemed necessary to assess the emergence of disease

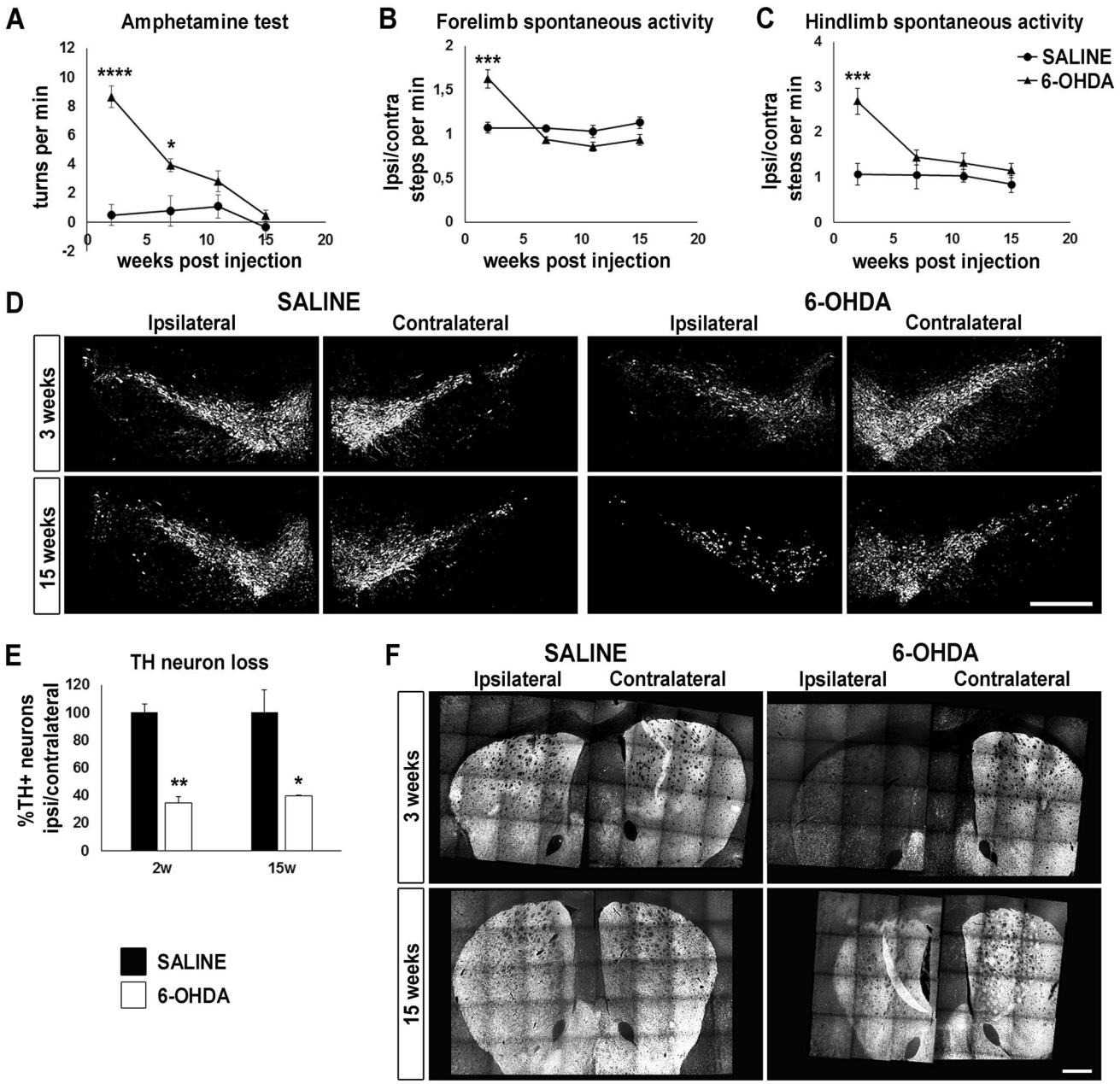

Fig. 4 Behavioral and immunohistochemical characterization of the 6-OHDA lesion model in NOD/SCID mice. **a** Amphetamine-induced rotational asymmetry in 6-OHDA- and saline-injected control mice. Data (turns/min) represent mean ± SEM (6-OHDA 8.64 ± 0.76; n = 16; saline 0.48 ± 0.72 turns per min; n = 13; ****P = 2.25×10^{-8} at 2 weeks; 6-OHDA 3.93 ± 0.43, n = 5; saline 0.78 ± 1.02 turns per min, n = 6; *P = 0.025 at 7 weeks). **b, c** Spontaneous forelimb (**b**) and hindlimb (**c**) activity showing ipsilateral versus contralateral paw preference (forelimbs: 6-OHDA 1.63 ± 0.10 ipsi/contralateral steps per min, n = 12; saline 1.07 ± 0.06, n = 6; ***P = 0.0002 at 2 weeks; 6-OHDA 0.94 ± 0.03 n = 4; saline 1.06 ± 0.03, n = 4; *P = 0.037 at 7 weeks; hindlimbs: 6-OHDA 2.68 ± 0.29, n = 10; saline 1.07 ± 0.24, n = 6;***P = 0.0007 at 2 weeks). **d** Representative confocal images of coronal midbrain sections immunostained for TH (from − 2.74 to − 3.06 mm from bregma) at 3 and 15 weeks after saline or 6-OHDA injection. A marked reduction of TH^+ neurons is evident in the ipsilateral side of 6-OHDA lesioned mice at both time points. Quantification is shown in (**e**) (65.5% loss of TH neurons, n = 3 per group **P = 0.0011 in 2 weeks, 60.2% loss, n = 3 per group *P = 0.0224 at 15 weeks). Scale bar, 500 µm. **f** Representative confocal images of coronal striatal sections showing TH innervation (+ 0.945 mm from bregma, next to injection level) at 3 and 15 weeks after saline or 6-OHDA injection. Denervation at 3 weeks followed by re-innervation at 15 weeks is apparent in the ipsilateral side of 6-OHDA lesioned animals. Scale bar, 500 µm

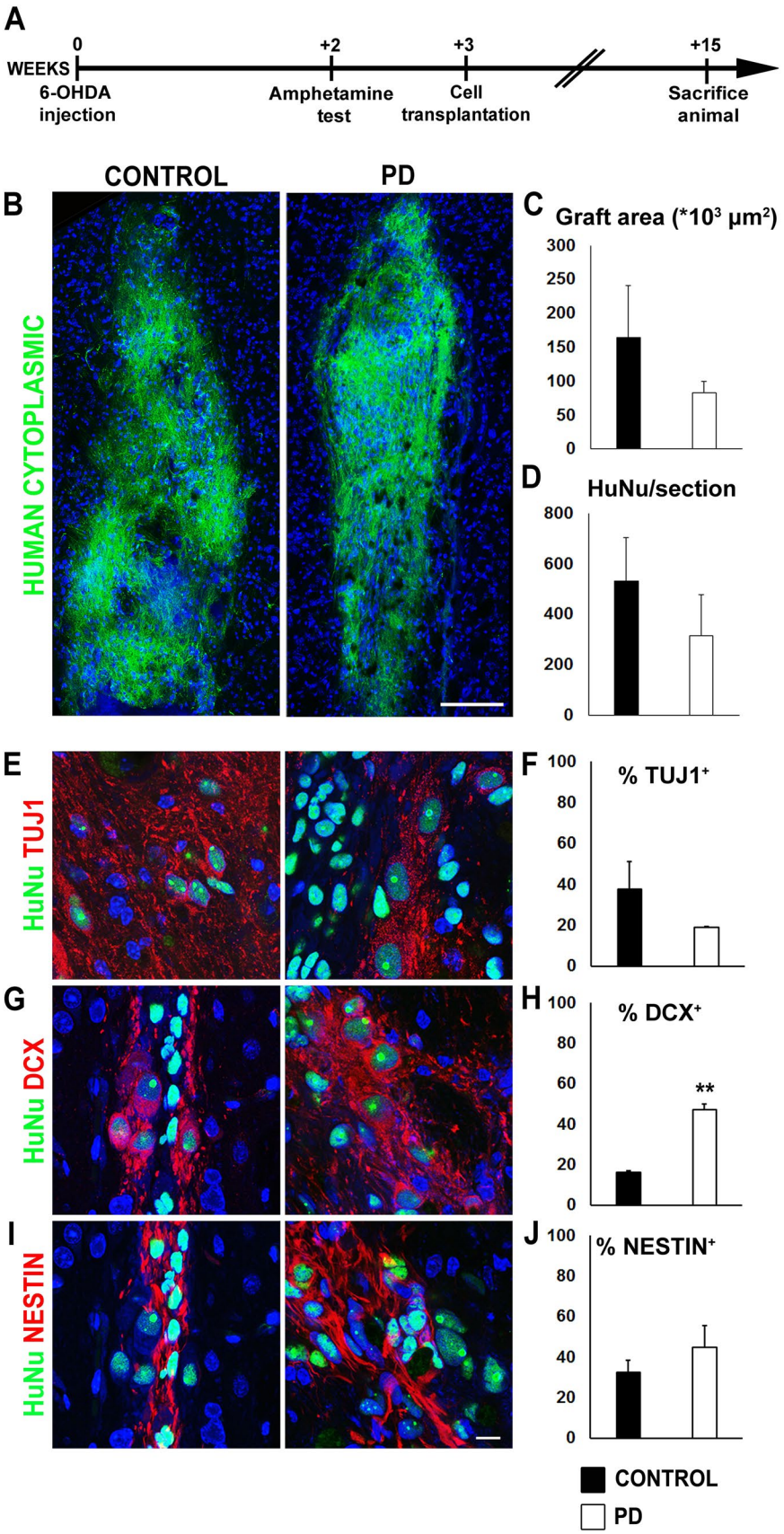

Fig. 5 In vivo engraftment of iPSC-derived control and PD cells. **a** Schematic drawing of the time course of the in vivo experiment. Cells were stereotactically transplanted 2 days after MACS enrichment (30DIV), as illustrated in Fig. 1. **b** Immunostaining for the human-specific cytoplasmic antigen (green) in control and PD-derived grafts. Nuclei are shown in blue. Scale bar, 100 µm. **c** Quantification of graft area (control $164.48 \pm 83.52 \times 10^3$ µm^2, n = 5; PD $76.68 \pm 15.7 \times 10^3$ µm^2, n = 3; P = 0.359) and **d** quantification of human nuclei (HuNu/section) (control 543.66 ± 182.14, n = 5; PD 279.06 ± 180.33, n = 3; P = 0.349). **e** Double immunostaining for HuNu (green) and TUJ1 (red); **f** Quantification of TUJ1$^+$/ HuNu$^+$ cells out of total HuNu$^+$ cells (control 37.59 ± 13.44%, n = 5; PD 19.09 ± 0.28%, n = 3; P = 0.2406). **g** Double immunostaining for HuNu (green) and DCX (red); **h** Quantification of DCX$^+$/ HuNu$^+$ cells out of total HuNu$^+$ cells (control 16.07 ± 0.89%, n = 5; PD 47.28 ± 2.88%, n = 3; ** P = 0.0091). **i** Double immunostaining for HuNu (green) and Nestin (red); **j** Quantification of Nestin$^+$/ HuNu$^+$ cells out of total HuNu$^+$ cells (control 32.64 ± 5.81%, n = 5; PD 44.72 ± 10.68%, n = 3; P = 0.3936). Total nuclei (of host tissue and graft) are shown in blue (DAPI staining). Scale bar (**e, g, i**), 10 µm. Data represent mean ± SEM

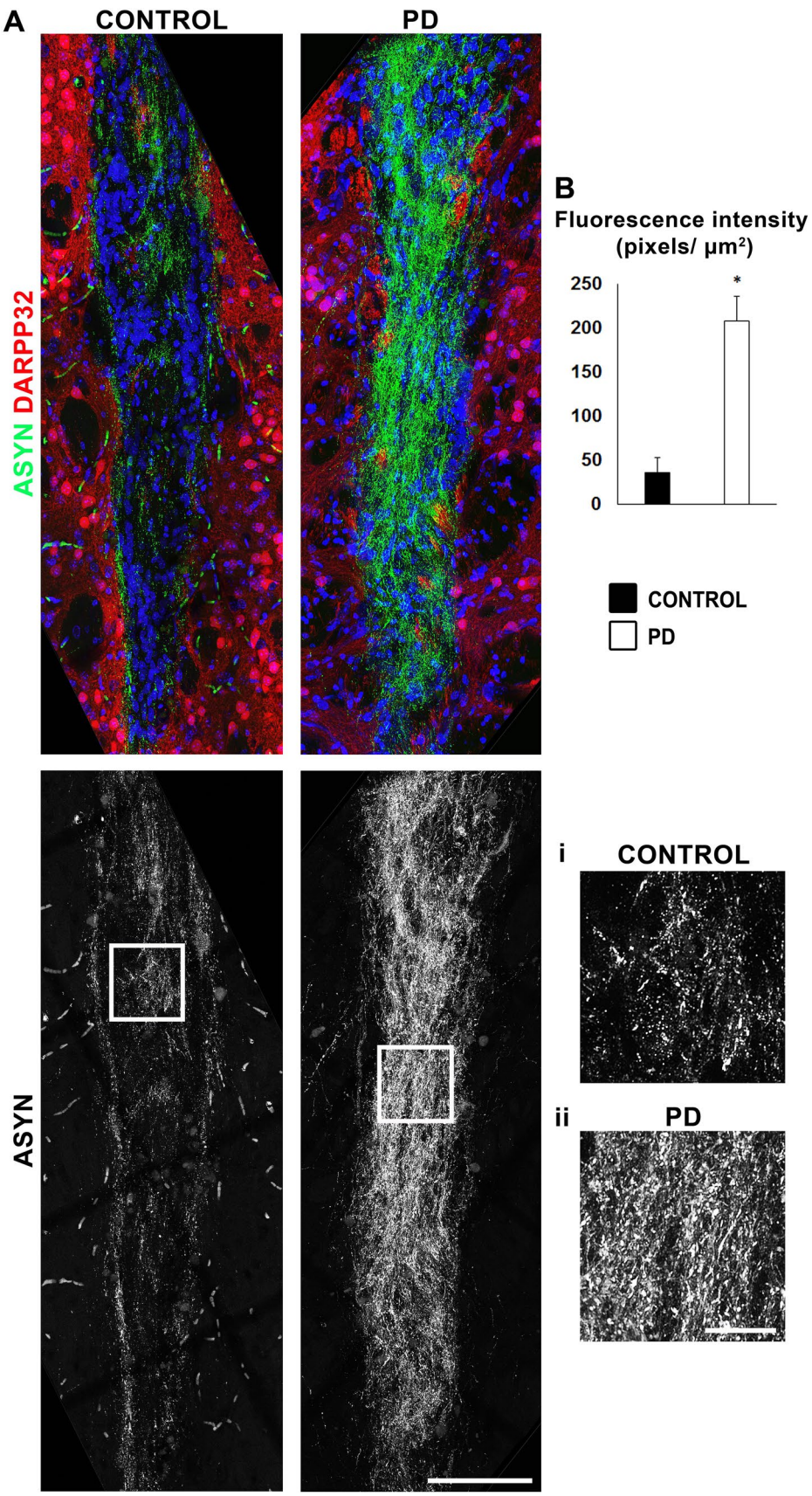

Fig. 6 Increased α-synuclein (αSyn) expression in grafted iPSC-derived PD neurons. **a** Representative images of striatal sections from mice that received control or PD-derived grafts, labeled for human αSyn (green, top panel; same fields: white lower panel). Host DARPP32^{+} medium spiny neurons are stained in red and nuclei are shown in blue (DAPI staining). Increased levels of αSyn immunoreactivity are clearly detected in PD-derived grafts. Scale bar, 100 µm. The insets in the lower panel are shown at higher magnification in (i, ii; αSyn, white). Scale bar in the insets, 25 µm. **b** Quantification of aSyn fluorescence intensity in control and PD-derived grafts (control 36.744 ± 16.825 pixels/ µm^2, n = 3; PD 207.389 ± 28.466 pixels/µm^2, n = 3; *P = 0.014). Data represent mean ± SEM

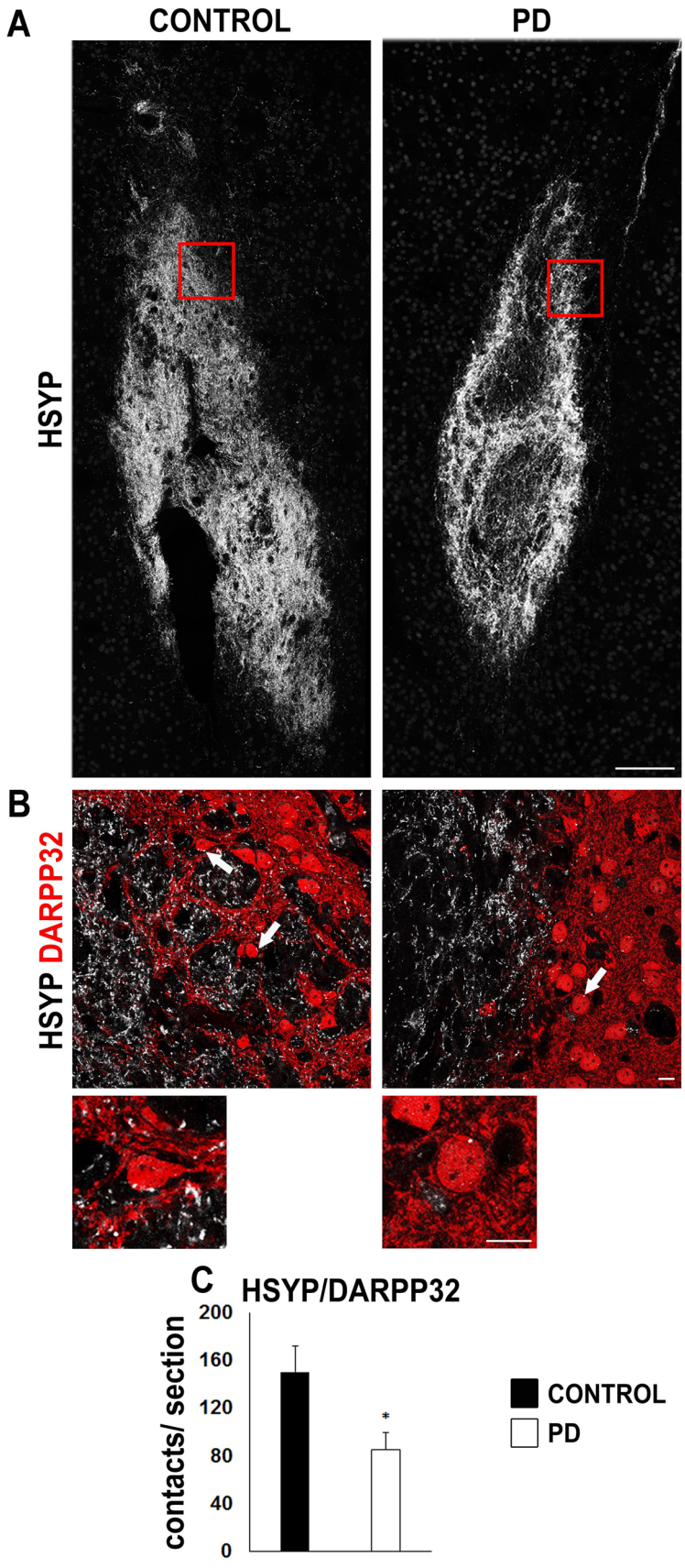

Fig. 7 Human synaptophysin immunoreactivity in PD and control-derived grafts in conjunction with DARP32 immunoreactivity of host medium spiny neurons. **a** Low power view of control and PD-derived grafts immunostained for human synaptophysin (HSYP; white). Scale bar, 100 µm. **b** At higher magnification (insets in **a**), double labeling for HSYP (white) and DARPP32 (red) indicates better integration of control-derived grafts within the host tissue. An intercalated control graft-host interphase is evident versus a sharply demarcated PD graft-host interphase. Arrows depict possible synaptic contacts between grafted cells and host neurons (also shown at higher magnification). Scale bars, 10 µm. **c** Quantification of HSYP/DARPP32 contacts per section in control and PD-derived grafts (150.6 ± 21.39, n = 5; PD 85.07 ± 14.73, n = 3;*P = 0.045). Data represent mean ± SEM

phenotypes in our cultures. in vitro characterization revealed similar profiles between control and p.A53T cells at the time of their transplantation (30 DIV) in 6-OHDA lesioned immunodeficient mice. However in more prolonged cultures up to 70 DIV, PD cells displayed significant morphological and functional alterations. This analysis uncovered both novel and previously identified defective phenotypes. In particular, we showed here for the first time that DCX-positive neurons showed abnormal neurite patterning with increased primary and secondary branching. Moreover, TH-positive neurons exhibited distorted and fragmented neurites indicative of neurodegeneration, as previously reported [23]. DCX is a microtubule-associated protein known for its involvement in neuronal migration and, more particularly, in the maintenance of bipolar shape in migrating neurons [21]. DCX is also important for proper dendritic development and remodeling [50]. Interestingly, it has been shown that DCX-positive immature neurons with LRRK2 deficiency, a gene associated with monogenetic PD, exhibit extended neuritic development and more complex arborization [35], a phenotype similar to our current observations.

Intracellular protein aggregates were detected here in mature TH-positive neurons leading to overt degenerative traits, in agreement with our previous observations [23] and other reports [43, 44]. Interestingly though, protein aggregates could also be seen in immature DCX-positive cells, suggesting that pathology starts a lot earlier than anticipated and is not confined to mature neurons. It is possible that sequestration of aggregation-prone proteins may initially represent a cytoprotective effect in response to cellular stress, eventually leading to degeneration of more mature TH-positive cells.

Emerging evidence suggests that a number of underlying mechanisms in neurodegenerative diseases are closely linked to neuritic maintenance, synaptic transmission and neuronal connectivity. Our electrophysiological analysis showed similar active and passive membrane properties between control and PD cells, in agreement with our previous observations [23]. Yet calcium imaging in p.A53T-neurons that was performed here for the first time, revealed higher frequency and amplified calcium transients, which is likely to impact on the identified phenotypes of p.A53T cells. It is known that calcium oscillations play critical roles in neuronal development and differentiation affecting neurite outgrowth and the formation of synaptic connections [42, 58]. Previous studies have shown calcium dysregulation in hiPSC-derived neurons from PD patients carrying the LRRK2 G2019S mutation [47] or mutations in the PD-linked gene GBA1 [46] as well as in hiPSC-derived neurons from patients with frontotemporal lobar degeneration tauopathy [15]. The observed altered network activity, along with the aberrant neurite branching observed in PD neurons, are in line with a defect in synaptic maturation and plasticity [32].

We next addressed whether the in vitro observed vulnerability of p.A53T neurons would be retained in vivo. The 6-OHDA lesion that results in loss of nigral dopamine neurons has been first established in rats as a PD model [57] and later in mice due to development of a large number transgenic mouse models for PD studies [3, 41, 56]. The majority of studies engaging differentiated derivatives of human pluripotent stem cells for transplantation use immunosuppressed rodent models where integration and functionality are assessed both histologically and behaviorally. Our data from two different tests for evaluation of motor activity in the 6-OHDA lesioned NOD/SCID mice were rather unexpected. In both tests a significant restoration of behavioral deficits occurred spontaneously in mice without transplantation. We postulate the occurrence of extensive sprouting of undamaged dopaminergic fibers within the ipsilateral striatum or/and a cross-hemispheric contribution of dopaminergic fibers originating from the contralateral substantia nigra. Contrary to the long-standing belief that dopamine neurons project unilaterally, a recent study has demonstrated that dopamine neurons have cross-hemispheric projections with functional significance [9]. Most interestingly, and in support of our findings, the authors of this study showed that in animals with a unilateral 6-OHDA lesion, contralateral projections could be stimulated with amphetamine to evoke dopamine release in the lesioned striatum, raising concerns when using this experimental approach to evaluate the efficacy of transplanted cells in pre-clinical studies.

Subsequently we focused on immunohistochemical analysis of the graft and the surrounding host environment. Assessment of the graft at 12 weeks after transplantation suggested that both control and PD cells survived and could differentiate to a similar extent despite the pathological features that these cells displayed in vitro. One difference we noted was an increased number of DCX-positive cells in PD grafts, suggesting that PD neurons might be stalled at this immature differentiation state, an observation that might account for their compromised ability to extend neurites and form contacts with host neurons. Considering the limited numbers of TH-positive neurons present in both control and PD grafts it is desirable to examine in future studies longer time points, exceeding 6 months after transplantation, which is a challenging task taking into consideration the increased mortality rate of the 6-OHDA lesioned NOD/SCID mice. Long-term studies are also needed to clarify whether the elevation in αSyn immunoreactivity seen in PD grafts (this study with p.A53T-αSyn grafts and [13] with LRRK2-G2019S grafts) - a phenotype that cannot be attributed to their more immature state - would eventually result in a pathological phenotype with formation of protein aggregates in mature neurons. Another issue is whether p.A53T pathology can spread from the graft to the host environment. Cell to cell seeding of αSyn and transmission of pathology

from patient to healthy human neurons has been recently observed in vitro [43]. Whether this may also occur in vivo remains to be seen. We speculate that graft-to-host transmission may require longer to emerge. An alternative possibility is that differences between human and mouse may prohibit αSyn transmission across species.

Despite similarities, the observed differences between control and PD grafts should not be overlooked as they may be intensified overtime affecting their integration within the tissue. Control-derived grafts tended to intermingle more efficiently at 12 weeks with the host tissue whilst PD grafts retained sharply demarcated boundaries. This was accompanied by a decreased number of PD graft-derived projections onto host medium spiny neurons. This may be explained either by an increased permissiveness of the host tissue to healthy human neurons or by the compromised ability of human PD neurons to form synaptic contacts in vivo as has been previously shown for these cells in vitro [23]. Under this light, further analysis of the phenotypes that patient cells acquire over longer periods of time as well as the use of multiple iPSC clones from different patients should extend our current proof-of-concept study and provide additional evidence for in vivo disease modeling.

Acknowledgements R.M. is grateful to Professor AJ Turner for mentorship and a life-long friendship. The authors thank Florentia Papastefanaki for constructive input throughout this study and help with figures and statistical analyses. This work was supported by: a grant from Stavros Niarchos Foundation to the Hellenic Pasteur Institute as part of the Foundation's initiative to support the Greek Research Center ecosystem, the Institut Pasteur PTR-523 grant and the project "A Greek Research Infrastructure for Visualizing & Monitoring Fundamental Biological Processes" (MIS 5002755) implemented under the Action for Reinforcement of Research and Innovation Infrastructure funded by the Operational Program "Competitiveness, Entrepreneurship and Innovation" (NSRF 2014–2020) and co-financed by Greece and the European Union (European Regional Development Fund). O.Z. was awarded a scholarship from the State Scholarship Foundation (IKY) funded by the Action "Scholarships for post-graduate studies" (Operational Program "Education and Lifelong learning", 2014–2020) and co-financed by the European Social Fund and the Greek government.

References

1. Barker RA, Parmar M, Studer L, Takahashi J (2017) Human trials of stem cell-derived dopamine neurons for Parkinson's disease: dawn of a new era. Cell Stem Cell 21(5):569–573
2. Behrstock S, Ebert AD, Klein S, Schmitt M, Moore JM, Svendsen CN (2008) Lesion-induced increase in survival and migration of human neural progenitor cells releasing GDNF. Cell Transplant 17(7):753–762
3. Brundin P, Isacson O, Gage FH, Prochiantz A, Bjorklund A (1986) The rotating 6-hydroxydopamine-lesioned mouse as a model for assessing functional effects of neuronal grafting. Brain Res 366(1–2):346–349
4. Byers B, Cord B, Nguyen HN, Schule B, Fenno L, Lee PC, Deisseroth K, Langston JW, Pera RR, Palmer TD (2011) SNCA triplication Parkinson's patient's iPSC-derived DA neurons accumulate alpha-synuclein and are susceptible to oxidative stress. PLoS ONE 6(11):e26159
5. Chartier-Harlin MC, Kachergus J, Roumier C, Mouroux V, Douay X, Lincoln S, Levecque C, Larvor L, Andrieux J, Hulihan M, Waucquier N, Defebvre L, Amouyel P, Farrer M, Destee A (2004) Alpha-synuclein locus duplication as a cause of familial Parkinson's disease. Lancet 364(9440):1167–1169
6. Cooper O, Seo H, Andrabi S, Guardia-Laguarta C, Graziotto J, Sundberg M, McLean JR, Carrillo-Reid L, Xie Z, Osborn T, Hargus G, Deleidi M, Lawson T, Bogetofte H, Perez-Torres E, Clark L, Moskowitz C, Mazzulli J, Chen L, Volpicelli-Daley L, Romero N, Jiang H, Uitti RJ, Huang Z, Opala G, Scarffe LA, Dawson VL, Klein C, Feng J, Ross OA, Trojanowski JQ, Lee VM, Marder K, Surmeier DJ, Wszolek ZK, Przedborski S, Krainc D, Dawson TM, Isacson O (2012) Pharmacological rescue of mitochondrial deficits in iPSC-derived neural cells from patients with familial Parkinson's disease. Sci Transl Med 4(141):141ra190
7. Devine MJ, Ryten M, Vodicka P, Thomson AJ, Burdon T, Houlden H, Cavaleri F, Nagano M, Drummond NJ, Taanman JW, Schapira AH, Gwinn K, Hardy J, Lewis PA, Kunath T (2011) Parkinson's disease induced pluripotent stem cells with triplication of the alpha-synuclein locus. Nat Commun 2:440
8. Doi D, Samata B, Katsukawa M, Kikuchi T, Morizane A, Ono Y, Sekiguchi K, Nakagawa M, Parmar M, Takahashi J (2014) Isolation of human induced pluripotent stem cell-derived dopaminergic progenitors by cell sorting for successful transplantation. Stem Cell Reports 2(3):337–350
9. Fox ME, Mikhailova MA, Bass CE, Takmakov P, Gainetdinov RR, Budygin EA, Wightman RM (2016) Cross-hemispheric dopamine projections have functional significance. Proc Natl Acad Sci USA 113(25):6985–6990
10. Glajch KE, Fleming SM, Surmeier DJ, Osten P (2012) Sensorimotor assessment of the unilateral 6-hydroxydopamine mouse model of Parkinson's disease. Behav Brain Res 230(2):309–316
11. Hargus G, Cooper O, Deleidi M, Levy A, Lee K, Marlow E, Yow A, Soldner F, Hockemeyer D, Hallett PJ, Osborn T, Jaenisch R, Isacson O (2010) Differentiated Parkinson patient-derived induced pluripotent stem cells grow in the adult rodent brain and reduce motor asymmetry in Parkinsonian rats. Proc Natl Acad Sci USA 107(36):15921–15926
12. Hargus G, Ehrlich M, Arauzo-Bravo MJ, Hemmer K, Hallmann AL, Reinhardt P, Kim KP, Adachi K, Santourlidis S, Ghanjati F, Fauser M, Ossig C, Storch A, Kim JB, Schwamborn JC, Sterneckert J, Scholer HR, Kuhlmann T, Zaehres H (2014) Origin-dependent neural cell identities in differentiated human iPSCs in vitro and after transplantation into the mouse brain. Cell Rep 8(6):1697–1703
13. Hemmer K, Smits LM, Bolognin S, Schwamborn JC (2017) In vivo phenotyping of Parkinson-specific stem cells reveals increased A-synuclein levels but no spreading. bioRxiv
14. Imaizumi Y, Okada Y, Akamatsu W, Koike M, Kuzumaki N, Hayakawa H, Nihira T, Kobayashi T, Ohyama M, Sato S, Takanashi M, Funayama M, Hirayama A, Soga T, Hishiki T, Suematsu M, Yagi T, Ito D, Kosakai A, Hayashi K, Shouji M, Nakanishi A, Suzuki N, Mizuno Y, Mizushima N, Amagai M, Uchiyama Y, Mochizuki H, Hattori N, Okano H (2012) Mitochondrial dysfunction associated with increased oxidative stress and alpha-synuclein accumulation in PARK2 iPSC-derived neurons and postmortem brain tissue. Mol Brain 5:35
15. Imamura K, Sahara N, Kanaan NM, Tsukita K, Kondo T, Kutoku Y, Ohsawa Y, Sunada Y, Kawakami K, Hotta A, Yawata S, Watanabe D, Hasegawa M, Trojanowski JQ, Lee VM, Suhara T, Higuchi M, Inoue H (2016) Calcium dysregulation contributes to neurodegeneration in FTLD patient iPSC-derived neurons. Sci Rep 6:34904

16. Katz LC, Shatz CJ (1996) Synaptic activity and the construction of cortical circuits. Science 274(5290):1133–1138
17. Kikuchi T, Morizane A, Doi D, Magotani H, Onoe H, Hayashi T, Mizuma H, Takara S, Takahashi R, Inoue H, Morita S, Yamamoto M, Okita K, Nakagawa M, Parmar M, Takahashi J (2017) Human iPS cell-derived dopaminergic neurons function in a primate Parkinson's disease model. Nature 548(7669):592–596
18. Kikuchi T, Morizane A, Doi D, Okita K, Nakagawa M, Yamakado H, Inoue H, Takahashi R, Takahashi J (2017) Idiopathic Parkinson's disease patient-derived induced pluripotent stem cells function as midbrain dopaminergic neurons in rodent brains. J Neurosci Res 95(9):1829–1837
19. Kim DS, Lee DR, Kim HS, Yoo JE, Jung SJ, Lim BY, Jang J, Kang HC, You S, Hwang DY, Leem JW, Nam TS, Cho SR, Kim DW (2012) Highly pure and expandable PSA-NCAM-positive neural precursors from human ESC and iPSC-derived neural rosettes. PLoS One 7(7):e39715
20. Kirkeby A, Grealish S, Wolf DA, Nelander J, Wood J, Lundblad M, Lindvall O, Parmar M (2012) Generation of regionally specified neural progenitors and functional neurons from human embryonic stem cells under defined conditions. Cell Rep 1(6):703–714
21. Koizumi H, Higginbotham H, Poon T, Tanaka T, Brinkman BC, Gleeson JG (2006) Doublecortin maintains bipolar shape and nuclear translocation during migration in the adult forebrain. Nat Neurosci 9(6):779–786
22. Koros C, Stamelou M, Simitsi A, Beratis I, Papadimitriou D, Papagiannakis N, Fragkiadaki S, Kontaxopoulou D, Papageorgiou SG, Stefanis L (2018) Selective cognitive impairment and hyposmia in p.A53T SNCA PD vs typical PD. Neurology 90(10):e864–e869
23. Kouroupi G, Taoufik E, Vlachos IS, Tsioras K, Antoniou N, Papastefanaki F, Chroni-Tzartou D, Wrasidlo W, Bohl D, Stellas D, Politis PK, Vekrellis K, Papadimitriou D, Stefanis L, Bregestovski P, Hatzigeorgiou AG, Masliah E, Matsas R (2017) Defective synaptic connectivity and axonal neuropathology in a human iPSC-based model of familial Parkinson's disease. Proc Natl Acad Sci USA 114(18):E3679–E3688
24. Koutsoudaki PN, Papastefanaki F, Stamatakis A, Kouroupi G, Xingi E, Stylianopoulou F, Matsas R (2016) Neural stem/progenitor cells differentiate into oligodendrocytes, reduce inflammation, and ameliorate learning deficits after transplantation in a mouse model of traumatic brain injury. Glia 64(5):763–779
25. Kriks S, Shim JW, Piao J, Ganat YM, Wakeman DR, Xie Z, Carrillo-Reid L, Auyeung G, Antonacci C, Buch A, Yang L, Beal MF, Surmeier DJ, Kordower JH, Tabar V, Studer L (2011) Dopamine neurons derived from human ES cells efficiently engraft in animal models of Parkinson's disease. Nature 480(7378):547–551
26. Kuijlaars J, Oyelami T, Diels A, Rohrbacher J, Versweyveld S, Meneghello G, Tuefferd M, Verstraelen P, Detrez JR, Verschuuren M, De Vos WH, Meert T, Peeters PJ, Cik M, Nuydens R, Brone B, Verheyen A (2016) Sustained synchronized neuronal network activity in a human astrocyte co-culture system. Sci Rep 6:36529
27. Lee DR, Yoo JE, Lee JS, Park S, Lee J, Park CY, Ji E, Kim HS, Hwang DY, Kim DS, Kim DW (2015) PSA-NCAM-negative neural crest cells emerging during neural induction of pluripotent stem cells cause mesodermal tumors and unwanted grafts. Stem Cell Rep 4(5):821–834
28. Lees AJ, Hardy J, Revesz T (2009) Parkinson's disease. Lancet 373(9680):2055–2066
29. Lin L, Goke J, Cukuroglu E, Dranias MR, VanDongen AM, Stanton LW (2016) Molecular Features Underlying Neurodegeneration Identified through in vitro modeling of genetically diverse Parkinson's disease patients. Cell Rep 15(11):2411–2426
30. Little D, Luft C, Mosaku O, Lorvellec M, Yao Z, Paillusson S, Kriston-Vizi J, Gandhi S, Abramov AY, Ketteler R, Devine MJ, Gissen P (2018) A single cell high content assay detects mitochondrial dysfunction in iPSC-derived neurons with mutations in SNCA. Sci Rep 8(1):9033
31. Liu S, Sawada T, Lee S, Yu W, Silverio G, Alapatt P, Millan I, Shen A, Saxton W, Kanao T, Takahashi R, Hattori N, Imai Y, Lu B (2012) Parkinson's disease-associated kinase PINK1 regulates miro protein level and axonal transport of mitochondria. PLoS Genet 8(3):e1002537
32. Lohmann C, Wong RO (2005) Regulation of dendritic growth and plasticity by local and global calcium dynamics. Cell Calcium 37(5):403–409
33. Nguyen HN, Byers B, Cord B, Shcheglovitov A, Byrne J, Gujar P, Kee K, Schule B, Dolmetsch RE, Langston W, Palmer TD, Pera RR (2011) LRRK2 mutant iPSC-derived DA neurons demonstrate increased susceptibility to oxidative stress. Cell Stem Cell 8(3):267–280
34. Papadimitriou D, Antonelou R, Miligkos M, Maniati M, Papagiannakis N, Bostantjopoulou S, Leonardos A, Koros C, Simitsi A, Papageorgiou SG, Kapaki E, Alcalay RN, Papadimitriou A, Athanassiadou A, Stamelou M, Stefanis L (2016) Motor and nonmotor features of carriers of the p.A53T alpha-synuclein mutation: a longitudinal study. Mov Disord 31(8):1226–1230
35. Paus M, Kohl Z, Ben Abdallah NM, Galter D, Gillardon F, Winkler J (2013) Enhanced dendritogenesis and axogenesis in hippocampal neuroblasts of LRRK2 knockout mice. Brain Res 1497:85–100
36. Petrucci S, Ginevrino M, Valente EM (2016) Phenotypic spectrum of alpha-synuclein mutations: new insights from patients and cellular models. Parkinsonism Relat Disord 22(Suppl 1):S16–S20
37. Polymeropoulos MH, Lavedan C, Leroy E, Ide SE, Dehejia A, Dutra A, Pike B, Root H, Rubenstein J, Boyer R, Stenroos ES, Chandrasekharappa S, Athanassiadou A, Papapetropoulos T, Johnson WG, Lazzarini AM, Duvoisin RC, Di Iorio G, Golbe LI, Nussbaum RL (1997) Mutation in the alpha-synuclein gene identified in families with Parkinson's disease. Science 276(5321):2045–2047
38. Puschmann A (2017) New genes causing hereditary Parkinson's disease or parkinsonism. Curr Neurol Neurosci Rep 17(9):66
39. Qiu L, Liao MC, Chen AK, Wei S, Xie S, Reuveny S, Zhou ZD, Hunziker W, Tan EK, Oh SKW, Zeng L (2017) Immature midbrain dopaminergic neurons derived from floor-plate method improve cell transplantation therapy efficacy for Parkinson's disease. Stem Cells Transl Med 6(9):1803–1814
40. Reinhardt P, Schmid B, Burbulla LF, Schondorf DC, Wagner L, Glatza M, Hoing S, Hargus G, Heck SA, Dhingra A, Wu G, Muller S, Brockmann K, Kluba T, Maisel M, Kruger R, Berg D, Tsytsyura Y, Thiel CS, Psathaki OE, Klingauf J, Kuhlmann T, Klewin M, Muller H, Gasser T, Scholer HR, Sterneckert J (2013) Genetic correction of a LRRK2 mutation in human iPSCs links parkinsonian neurodegeneration to ERK-dependent changes in gene expression. Cell Stem Cell 12(3):354–367
41. di Val Cervo PR, Romanov RA, Spigolon G, Masini D, Martin-Montanez E, Toledo EM, La Manno G, Feyder M, Pifl C, Ng YH, Sanchez SP, Linnarsson S, Wernig M, Harkany T, Fisone G, Arenas E (2017) Induction of functional dopamine neurons from human astrocytes in vitro and mouse astrocytes in a Parkinson's disease model. Nat Biotechnol 35(5):444–452
42. Rosenberg SS, Spitzer NC (2011) Calcium signaling in neuronal development. Cold Spring Harb Perspect Biol 3(10):a004259
43. Ryan SD, Dolatabadi N, Chan SF, Zhang X, Akhtar MW, Parker J, Soldner F, Sunico CR, Nagar S, Talantova M, Lee B, Lopez K, Nutter A, Shan B, Molokanova E, Zhang Y, Han X, Nakamura T, Masliah E, Yates JR III, Nakanishi N, Andreyev AY, Okamoto S, Jaenisch R, Ambasudhan R, Lipton SA (2013) Isogenic human iPSC Parkinson's model shows nitrosative stress-induced dysfunction in MEF2-PGC1 alpha transcription. Cell 155(6):1351–1364

44. Ryan T, Bamm VV, Stykel MG, Coackley CL, Humphries KM, Jamieson-Williams R, Ambasudhan R, Mosser DD, Lipton SA, Harauz G, Ryan SD (2018) Cardiolipin exposure on the outer mitochondrial membrane modulates alpha-synuclein. Nat Commun 9(1):817
45. Sanchez-Danes A, Richaud-Patin Y, Carballo-Carbajal I, Jimenez-Delgado S, Caig C, Mora S, Di Guglielmo C, Ezquerra M, Patel B, Giralt A, Canals JM, Memo M, Alberch J, Lopez-Barneo J, Vila M, Cuervo AM, Tolosa E, Consiglio A, Raya A (2012) Disease-specific phenotypes in dopamine neurons from human iPS-based models of genetic and sporadic Parkinson's disease. EMBO Mol Med 4(5):380–395
46. Schondorf DC, Aureli M, McAllister FE, Hindley CJ, Mayer F, Schmid B, Sardi SP, Valsecchi M, Hoffmann S, Schwarz LK, Hedrich U, Berg D, Shihabuddin LS, Hu J, Pruszak J, Gygi SP, Sonnino S, Gasser T, Deleidi M (2014) iPSC-derived neurons from GBA1-associated Parkinson's disease patients show autophagic defects and impaired calcium homeostasis. Nat Commun 5:4028
47. Schwab AJ, Ebert AD (2015) Neurite aggregation and calcium dysfunction in iPSC-derived sensory neurons with Parkinson's disease-related LRRK2 G2019S mutation. Stem Cell Rep 5(6):1039–1052
48. Seibler P, Graziotto J, Jeong H, Simunovic F, Klein C, Krainc D (2011) Mitochondrial Parkin recruitment is impaired in neurons derived from mutant PINK1 induced pluripotent stem cells. J Neurosci 31(16):5970–5976
49. Shen D, Coleman J, Chan E, Nicholson TP, Dai L, Sheppard PW, Patton WF (2011) Novel cell- and tissue-based assays for detecting misfolded and aggregated protein accumulation within aggresomes and inclusion bodies. Cell Biochem Biophys 60(3):173–185
50. Shin E, Kashiwagi Y, Kuriu T, Iwasaki H, Tanaka T, Koizumi H, Gleeson JG, Okabe S (2013) Doublecortin-like kinase enhances dendritic remodelling and negatively regulates synapse maturation. Nat Commun 4:1440
51. Simon-Sanchez J, Schulte C, Bras JM, Sharma M, Gibbs JR, Berg D, Paisan-Ruiz C, Lichtner P, Scholz SW, Hernandez DG, Kruger R, Federoff M, Klein C, Goate A, Perlmutter J, Bonin M, Nalls MA, Illig T, Gieger C, Houlden H, Steffens M, Okun MS, Racette BA, Cookson MR, Foote KD, Fernandez HH, Traynor BJ, Schreiber S, Arepalli S, Zonozi R, Gwinn K, van der Brug M, Lopez G, Chanock SJ, Schatzkin A, Park Y, Hollenbeck A, Gao J, Huang X, Wood NW, Lorenz D, Deuschl G, Chen H, Riess O, Hardy JA, Singleton AB, Gasser T (2009) Genome-wide association study reveals genetic risk underlying Parkinson's disease. Nat Genet 41(12):1308–1312
52. Soldner F, Hockemeyer D, Beard C, Gao Q, Bell GW, Cook EG, Hargus G, Blak A, Cooper O, Mitalipova M, Isacson O, Jaenisch R (2009) Parkinson's disease patient-derived induced pluripotent stem cells free of viral reprogramming factors. Cell 136(5):964–977
53. Stefanis L (2012) alpha-Synuclein in Parkinson's disease. Cold Spring Harb Perspect Med 2(2):a009399
54. Sundberg M, Bogetofte H, Lawson T, Jansson J, Smith G, Astradsson A, Moore M, Osborn T, Cooper O, Spealman R, Hallett P, Isacson O (2013) Improved cell therapy protocols for Parkinson's disease based on differentiation efficiency and safety of hESC-, hiPSC-, and non-human primate iPSC-derived dopaminergic neurons. Stem Cells 31(8):1548–1562
55. Taoufik E, Kouroupi G, Zygogianni O, Matsas R (2018) Synaptic dysfunction in neurodegenerative and neurodevelopmental diseases: an overview of induced pluripotent stem-cell-based disease models. Open Biol 8(9):180138
56. Thiele SL, Warre R, Nash JE (2012) Development of a unilaterally-lesioned 6-OHDA mouse model of Parkinson's disease. J Vis Exp. https://doi.org/10.3791/3234
57. Ungerstedt U (1968) 6-Hydroxy-dopamine induced degeneration of central monoamine neurons. Eur J Pharmacol 5(1):107–110
58. van Ooyen A, van Pelt J (1994) Activity-dependent neurite outgrowth and neural network development. Prog Brain Res 102:245–259
59. Von Voigtlander PF, Moore KE (1973) Involvement of nigro-striatal neurons in the in vivo release of dopamine by amphetamine, amantadine and tyramine. J Pharmacol Exp Ther 184(3):542–552
60. Wrasidlo W, Tsigelny IF, Price DL, Dutta G, Rockenstein E, Schwarz TC, Ledolter K, Bonhaus D, Paulino A, Eleuteri S, Skjevik AA, Kouznetsova VL, Spencer B, Desplats P, Gonzalez-Ruelas T, Trejo-Morales M, Overk CR, Winter S, Zhu C, Chesselet MF, Meier D, Moessler H, Konrat R, Masliah E (2016) A de novo compound targeting alpha-synuclein improves deficits in models of Parkinson's disease. Brain 139(Pt 12):3217–3236
61. Zhang LI, Poo MM (2001) Electrical activity and development of neural circuits. Nat Neurosci 4(11 Suppl):1207–1214
62. Zhang P, Xia N, Pera Reijo RA (2014) Directed dopaminergic neuron differentiation from human pluripotent stem cells. J Vis Exp 91:51737